

Time-Crystalline Phase in a Single-Band Holographic Superconductor

Chi-Hsien Tai* and Wen-Yu Wen†

*Department of Physics and Center for Theoretical Physics,
Chung Yuan Christian University, Taoyuan, Taiwan*

Abstract

We investigate the emergence of a time-crystalline phase in a single-band holographic superconductor, extending the AdS/CFT framework. By incorporating a nonlinear gauge-scalar coupling and external driving, we derive coupled equations of motion for the plasma and Higgs modes, analogous to those in high- T_c superconductors. Multi-scale analysis reveals a sum resonance with subharmonic growth indicating broken time-translation symmetry. We perform numerical computation of quasinormal mode and demonstrate the transition to the time-crystalline phase. The holographic model may serve as a robust tool for studying strongly coupled time crystals.

*Electronic address: xkp92214@gmail.com

†Electronic address: wenw@cycu.edu.tw

I. INTRODUCTION

Time crystals represent a novel phase of matter that spontaneously breaks time-translation symmetry, manifesting as periodic motion in the absence of external periodic driving. This concept, originally proposed as a theoretical curiosity, has evolved into a vibrant area of research bridging condensed matter physics, quantum optics, and non-equilibrium statistical mechanics. The idea was first introduced as an extension of spatial crystals to the time domain, where a system in its ground state exhibits periodic behavior without energy input [1, 2]. However, early proposals faced challenges related to no-go theorems in equilibrium systems, leading to refinements that emphasized non-equilibrium, driven, or Floquet-engineered setups [3, 4]. Over the past decade, time crystals have been realized experimentally in diverse platforms, including trapped ions, ultracold atoms, and spin chains, where discrete time-translation symmetry breaking leads to subharmonic responses stable against perturbations [5, 6].

In high-T_c superconductors, recent experimental and theoretical advances have uncovered signatures of time-crystalline behavior arising from the nonlinear coupling between collective modes under optical driving [7]. Specifically, the interplay between the Higgs mode, corresponding to amplitude fluctuations of the superconducting order parameter, and the Josephson plasma mode, associated with phase oscillations, has been shown to generate subharmonic responses when resonantly driven, a hallmark of discrete time-crystal formation. These phenomena have been observed in materials like cuprates and iron-based superconductors, where ultrafast laser pulses induce coherent oscillations that persist beyond thermal relaxation times [8, 9]. Theoretical models, often based on lattice simulations or effective field theories, highlight how parametric resonances amplify these modes, leading to long-lived periodic states that challenge traditional notions of dissipation in open systems [10]. Persistent multi-frequency dynamics of superconducting order parameters are noted in related studies, suggesting potential applications in quantum information processing and non-equilibrium control [11].

To model such strongly coupled, driven many-body systems, the framework of holographic duality, as pioneered by Hartnoll et al. [12], provides a powerful tool. By leveraging the Anti-de Sitter/Conformal Field Theory (AdS/CFT) correspondence, a gravitational description in the bulk can be mapped onto a strongly interacting boundary theory, here representing a

superconducting state. This approach naturally captures emergent phenomena in strongly correlated systems where traditional perturbative methods fail, such as near quantum critical points or in the presence of strong electron-phonon interactions [13]. Holography has successfully modeled high-T_c superconductivity features, including pseudogap phases and strange metal behavior, by treating the dual gravity theory as a mean-field approximation to quantum many-body physics.

In this work, we extend the single-band holographic superconductor model to explicitly exhibit time-crystalline dynamics. We introduce a nonlinear interaction term between the scalar (order parameter) and gauge fields, incorporate external optical driving, and derive an effective equation of motion (EOM) for the coupled mode system. Using multi-scale analysis, we estimate sharp resonance conditions where the driven system enters a time-crystalline phase. These analytical predictions are corroborated by extensive numerical simulations of the full nonlinear EOMs, revealing the existence of subharmonic peaks. By bridging lattice-based simulations of high-T_c superconductors with holographic methods, our model offers insights into universal mechanisms of time-crystal formation in strongly coupled systems, potentially guiding future experiments in optically pumped quantum materials [14].

Our results not only confirm the emergence of a driven time crystal in a holographically dual superconductor but also provide a controlled theoretical laboratory for exploring non-equilibrium symmetry breaking in strongly correlated matter. These findings bridge optical control of quantum materials with gravitational descriptions of criticality, offering new insights into the universal features of dynamic phases under periodic driving.

II. BULK MODEL AND CONDENSED BACKGROUND

We adopt the probe limit Abelian Higgs action [12], which reads

$$S = \int d^4x \sqrt{-g} \left[R + \frac{6}{L^2} - \frac{1}{4} F_{\mu\nu} F^{\mu\nu} - |D_\mu \psi|^2 - m^2 |\psi|^2 \right]. \quad (1)$$

Although the scalar field ψ and $U(1)$ gauge field A behaves like those in the usual Ginzburg-Landau theory, their asymptotic expansion at the boundary encodes physical quantities, such as the condensation, chemical potential and charge density, in the dual field theory.

We work in the planar AdS_4 black-brane geometry:

$$ds^2 = \frac{L^2}{u^2} \left(-f(u) dt^2 + \frac{du^2}{f(u)} + dx^2 + dy^2 \right), \quad f(u) = 1 - u^3/u_+^3, \quad (2)$$

with radial coordinate $u \in (0, u_+)$, where boundary at $u \rightarrow 0$ and future horizon at $u \rightarrow u_+$. For simplicity, we set radius of curvature $L = 1$ and horizon $u_+ = 1$ throughout the paper. The Hawking temperature, $T = 3/4\pi$, also characterizes the critical temperature below which condensation occurs in the dual superconductor.

We take the condensed static background in radial gauge $A_u = 0$:

$$A = \phi_0(u) dt, \quad \psi = \psi_0(u) \in \mathbb{R}, \quad (3)$$

obeying the coupled ODEs

$$\psi_0'' + \left(\frac{f'}{f} - \frac{2}{u} \right) \psi_0' + \left(\frac{q^2 \phi_0^2}{f^2} - \frac{m^2}{u^2 f} \right) \psi_0 = 0, \quad (4)$$

$$\phi_0'' - \frac{2}{u} \phi_0' - \frac{2q^2 \psi_0^2}{u^2 f} \phi_0 = 0. \quad (5)$$

Regularity at the horizon enforces $\phi_0(1) = 0$, while near the boundary we have the asymptotics

$$\psi_0(u) = \psi^{(1)} u + \psi^{(2)} u^2 + \dots, \quad \phi_0(u) = \mu - \rho u + \dots, \quad (6)$$

where we choose $m^2 = -2$ and $\psi^{(1)} = 0$ for a source free condensate in standard quantization. μ and ρ are chemical potential and charge density.

III. LINEAR EXCITATIONS AND QUASINORMAL MODES AT $k = 0$

G. Homann et al. [7] proposes a light-induced time crystalline state in a high- T_c superconductor, advancing light control toward non-equilibrium orders and further time crystals in the solid-state domain. It characterizes this state by a time crystal spontaneously breaking time-translation symmetry with subharmonic response.

Termed a Higgs time crystal, it arises from coupled Higgs and Josephson plasma modes in a superconductor with broken $U(1)$ symmetry and an amplitude oscillation order parameter, as in $|\psi|^4$ theory. The Higgs mode h (amplitude fluctuation) and Josephson plasma mode a (phase oscillation) are orthogonal due to induced electromagnetic interactions. Mapping onto optically driven high- T_c superconductors as a function of driving frequency ω_d and

amplitude E_0 , non-linear coupling $\sim a^2 h$ at $\omega_d = \omega_H + \omega_J$ yields the time crystalline phase, with ω_H (Higgs) and ω_J (plasma) frequencies. Persistent multi-frequency dynamics of superconducting order parameters are noted in related studies.

In the standard holographic construction, it is sufficient for simple mass term to stabilize the condensate vacuum without introduction of $|\psi|^4$ term. This is mainly because scalar fields in the AdS space admits solutions for some $m^2 < 0$. The Higgs mode and plasma mode come naturally from perturbation of gauge field δA and $\delta\psi$ in the superconducting phase. The coupling between two modes arises from radial reduction of terms like $|D\psi|^2$. The Maxwell on-shell variation provides the boundary term $\int dt A_x^{(0)} \delta\langle j_x \rangle$, so injects the drive in the reduced description. At last, our dynamics has dissipation due to ingoing flux at the horizon. In linear response, this corresponds to the imaginary part of quasi-normal mode (QNM). In the following, we will derive each terms in the desired coupled EOMs from the model of holographic superconductor.

A. Transverse gauge (plasma) sector A_x

The quadratic Maxwell Lagrangian density for a homogeneous transverse mode at $k = 0$ is

$$\mathcal{L}_J^{(2)} = \frac{1}{2}\sqrt{-g}\left[(-g^{tt})g^{xx}(\partial_t A_x)^2 - g^{uu}g^{xx}(\partial_u A_x)^2\right] - \frac{1}{2}\sqrt{-g}\frac{2q^2\psi_0^2}{u^2 f} A_x^2. \quad (7)$$

Using the metric factors gives

$$\mathcal{L}_J^{(2)} = \frac{1}{2}\frac{(\partial_t A_x)^2}{f} - \frac{1}{2}f(\partial_u A_x)^2 - \frac{1}{2}\frac{2q^2\psi_0^2}{u^2 f} A_x^2. \quad (8)$$

Project with $A_x(u, t) = a_x(t)Y_J(u)$. The time-kinetic term reduces to

$$\int_0^1 du \frac{1}{2}\frac{(\partial_t A_x)^2}{f} = \frac{1}{2}\dot{a}_x^2 \int_0^1 du \frac{|Y_J|^2}{f} \equiv \frac{1}{2}\dot{a}_x^2, \quad (9)$$

when we *normalize*

$$\int_0^1 du \mathcal{W}_J |Y_J|^2 = 1, \quad \mathcal{W}_J(u) := \sqrt{-g}(-g^{tt})g^{xx} = \frac{1}{f(u)}. \quad (10)$$

The remaining quadratic potential is

$$-\frac{1}{2}a_x^2 \int_0^1 du \left[f(Y_J')^2 + \frac{2q^2\psi_0^2}{u^2 f} Y_J^2 \right]. \quad (11)$$

Multiply the QNM equation (21) by f to obtain the Sturm–Liouville form

$$(fY'_J)' + \left(\frac{\omega^2}{f} - \frac{2q^2\psi_0^2}{u^2} \right) Y_J = 0. \quad (12)$$

Further multiplying by Y_J and integrating over u , boundary terms vanish by the QNM boundary conditions (ingoing horizon, no source at the boundary), yielding

$$\int_0^1 du \left[f(Y'_J)^2 + \frac{2q^2\psi_0^2}{u^2} Y_J^2 \right] = \omega_J^2 \int_0^1 du \frac{Y_J^2}{f}. \quad (13)$$

With the normalization above, the potential reduces to $-\frac{1}{2}\omega_J^2 a_x^2$. Hence

$$L_J^{(2)} = \frac{1}{2}\dot{a}_x^2 - \frac{1}{2}\omega_J^2 a_x^2. \quad (14)$$

B. Higgs (amplitude) sector $\eta = \delta\psi$

The quadratic scalar–gauge Lagrangian density at $k = 0$ reads

$$\mathcal{L}_H^{(2)} = \frac{1}{2}\sqrt{-g}(-g^{tt})(\partial_t\eta)^2 - \frac{1}{2}\sqrt{-g}g^{uu}(\partial_u\eta)^2 - \frac{1}{2}\sqrt{-g}\left(\frac{m^2}{u^2} + \frac{q^2\phi_0^2}{f}\right)\eta^2 \quad (15)$$

$$- \sqrt{-g}\frac{2q^2\phi_0\psi_0}{f}\eta\varphi - \frac{1}{2}\sqrt{-g}\frac{2q^2\psi_0^2}{u^2f}\varphi^2, \quad (16)$$

with $\varphi = \delta A_t$. Using the metric factors gives the time–kinetic weight

$$\mathcal{W}_H(u) := \sqrt{-g}(-g^{tt}) = \frac{1}{u^2 f(u)}. \quad (17)$$

Project with $\eta(u, t) = h(t)Y_H(u)$. Then

$$\int_0^1 du \frac{1}{2}\mathcal{W}_H(\partial_t\eta)^2 = \frac{1}{2}\dot{h}^2 \int_0^1 du \mathcal{W}_H|Y_H|^2 \equiv \frac{1}{2}\dot{h}^2, \quad (18)$$

after normalizing $\int_0^1 du \mathcal{W}_H|Y_H|^2 = 1$.

Because η mixes with φ , the correct potential follows from the coupled QNM eigen problem. Let $U = (Y_H, \Phi)^T$ solve the Higgs system with QNM boundary conditions. A similar integration by parts then gives

$$\int_0^1 du \left\{ \frac{f}{u^2}|Y'_H|^2 + \frac{1}{u^2}\left(m^2 + \frac{q^2\phi_0^2}{f}\right)|Y_H|^2 + \frac{2q^2\phi_0\psi_0}{u^2f}\Re(Y_H^*\Phi) + \frac{q^2\psi_0^2}{u^2f}|\Phi|^2 \right\} = \omega_H^2 \int_0^1 du \frac{|Y_H|^2}{u^2 f}. \quad (19)$$

With the chosen normalization, the quadratic potential reduces to $-\frac{1}{2}\omega_H^2 h^2$. Hence

$$L_H^{(2)} = \frac{1}{2}\dot{h}^2 - \frac{1}{2}\omega_H^2 h^2. \quad (20)$$

C. Damping from horizon flux

Linear QNMs decay as $e^{-i\omega t}$ with complex $\omega = \Omega - i\Gamma/2$. The retarded time-domain dynamics is reproduced by including a Rayleigh functional ¹ $\mathcal{R} = \frac{1}{2}\gamma_J \dot{a}_x^2 + \frac{1}{2}\gamma_H \dot{h}^2$ with $\gamma_{J/H} = -2\Im \omega_{J/H}^{\text{QNM}}$. We present QNMs for each mode as follows:

- Transverse gauge (plasma) mode

With $\delta A_x(u, t) = \Re\{Y_J(u) e^{-i\omega t}\}$ and other components unperturbed, the linearized Maxwell equation gives

$$Y_J'' + \frac{f'}{f} Y_J' + \left(\frac{\omega^2}{f^2} - \frac{2q^2\psi_0^2}{u^2 f} \right) Y_J = 0. \quad (21)$$

Quasinormal boundary conditions are: ingoing at the horizon, implying $Y_J \propto (1 - u)^{-i\omega/(4\pi T)} = (1 - u)^{-i\omega/3}$, and no source at the boundary, saying $Y_J \sim u$. The resulting complex eigen frequency is denoted

$$\omega_J^{\text{QNM}} = \Omega_J - i\Gamma_J/2, \quad (22)$$

where $\omega_J \equiv \Re \omega_J^{\text{QNM}} = \Omega_J$, $\gamma_J \equiv -2\Im \omega_J^{\text{QNM}} = \Gamma_J$.

- Higgs (amplitude) mode

In radial gauge $\delta A_u = 0$ and with real background phase, we consider $\delta\psi(u, t) = \eta(u) e^{-i\omega t}$ and $\delta A_t(u, t) = \varphi(u) e^{-i\omega t}$. The coupled linear system is

$$\eta'' + \left(\frac{f'}{f} - \frac{2}{u} \right) \eta' + \left(\frac{\omega^2}{f^2} + \frac{q^2\phi_0^2}{f^2} - \frac{m^2}{u^2 f} \right) \eta + \frac{2q^2\phi_0\psi_0}{f^2} \varphi = 0, \quad (23)$$

$$\varphi'' - \frac{2}{u} \varphi' - \frac{2q^2\psi_0^2}{u^2 f} \varphi - \frac{4q^2\phi_0\psi_0}{u^2 f} \eta = 0. \quad (24)$$

Boundary conditions: ingoing for $\eta \propto (1 - u)^{-i\omega/3}$, regular φ at the horizon; at the boundary, no scalar source and $\varphi(0) = 0$ (no chemical potential modulation). The complex eigen frequency $\omega_H^{\text{QNM}} = \Omega_H - i\Gamma_H/2$ defines $\omega_H = \Omega_H$ and $\gamma_H = \Gamma_H$.

D. Mode coupling and effective boundary ODEs

We remark that time-crystalline behavior arises from the nonlinear coupling between collective modes. In this section, we show that two effective couplings in boundary ODEs can be obtained by dimensional reduction from bulk geometry.

¹ We direct readers to appendix A for relation between Rayleigh functional and QNMs.

- Higgs pumping coefficient g (enters the h -equation). Recall that we work in radial gauge $A_u = 0$ and set

$$\psi = \psi_0(u) + \eta(u, t), \quad A_t = \phi_0(u) + \varphi(u, t), \quad A_x(u, t) = a_x(t) Y_J(u), \quad \eta(u, t) = h(t) Y_H(u).$$

From the bulk scalar kinetic term $-|D\psi|^2$, keeping terms up to *third* order in the small fluctuations $\{\eta, \varphi, A_x\}$ gives the cubic term

$$\mathcal{L}_{\text{sc}}^{(3)} = -2q^2 \sqrt{-g} g^{xx} \psi_0 \eta A_x^2 + \dots \quad (25)$$

so projecting with the *Higgs* weight gives

$$g = \frac{2q^2 \int_0^1 du \sqrt{-g} g^{xx} \psi_0 Y_H |Y_J|^2}{\int_0^1 du \sqrt{-g} (-g^{tt}) |Y_H|^2}. \quad (26)$$

This yields the nonlinear drive $g a_x^2$ in

$$\ddot{h} + \gamma_H \dot{h} + \omega_H^2 h + \boxed{g a_x^2} = 0. \quad (27)$$

- Spring-modulation coefficient χ (enters the a_x -equation). In the quadratic Maxwell sector, $-|D\psi|^2$ contributes an A_x “mass kernel”

$$\mathcal{M}_{A_x}(u) = \frac{2q^2 \psi^2}{u^2 f}.$$

Linearizing the A_x mass kernel with respect to the Higgs fluctuation ²,

$$\delta \left(\frac{2q^2 \psi^2}{u^2 f} \right) A_x^2 = \left(\frac{4q^2 \psi}{u^2 f} \right) \delta \psi A_x^2 = \left(\frac{4q^2 \psi_0}{u^2 f} \right) \eta A_x^2,$$

and projecting with the *gauge* weight gives

$$\chi = \frac{\int_0^1 du \sqrt{-g} \left(-\frac{4q^2 \psi_0}{u^2 f} \right) Y_H |Y_J|^2}{\int_0^1 du \sqrt{-g} (-g^{tt}) g^{xx} |Y_H|^2}. \quad (28)$$

It appears as a spring modulation in

$$\ddot{a}_x + \gamma_J \dot{a}_x + \left(\omega_J^2 + \boxed{\chi h} \right) a_x = J \cos(\omega_d t). \quad (29)$$

² We comment that an extra $+\alpha |\psi|^2 A_\mu A^\mu$, if added in the action, can also contribute $+4\alpha u^2 \psi_0 \eta A_x$.

We note that g and χ come from different bulk operators and are projected with different kinetic *weights*. Since those weights are associated with QNMs (dissipation at horizon), the reduction is non-Hermitian; hence they cannot be derived *simultaneously* from single conservative term like $\propto a_x^2 h$ in the effective action. In other words, holographically, they are generically unrelated. Later, we will show, in principle, they can be individually rescaled.

IV. MULTIPLE-SCALE ANALYSIS AND EVENLOPES

Start with the boundary ODEs collected from previous section:

$$\ddot{a}_x + \gamma_J \dot{a}_x + \omega_J^2 a_x + \chi h a_x = j_0 \cos(\omega_d t), \quad (30)$$

$$\ddot{h} + \gamma_H \dot{h} + \omega_H^2 h + g a_x^2 = 0. \quad (31)$$

Assume in a weakly driven and coupled regime, we introduce a small bookkeeping parameter

$$j_0 = \varepsilon J, \quad g = \varepsilon G, \quad \chi = \varepsilon C,$$

and define a slow time $T = \varepsilon t$. We seek following near resonant responses

$$\omega_d = \omega_J + \varepsilon \sigma_J, \quad 2\omega_d = \omega_H + \varepsilon \sigma_H^{(2:1)}, \quad \omega_d = \omega_J + \omega_H + \varepsilon \sigma_H^{(\text{sum})}.$$

We first assume the fields can be written as fast carrier oscillations with slow envelopes:

$$a_x(t) = A(T) e^{i\omega_d t} + \bar{A}(T) e^{-i\omega_d t}, \quad h(t) = H(T) e^{i\Omega t} + \bar{H}(T) e^{-i\Omega t}, \quad (32)$$

where $\Omega = \omega_H$ for the **2 : 1** channel and $\Omega = \omega_d - \omega_J$ for the **sum** channel. Let dots denote t -derivatives and primes denote T -derivatives. We remark

$$\frac{d}{dt} = \partial_t + \varepsilon \partial_T, \quad \frac{d^2}{dt^2} = \partial_t^2 + 2\varepsilon \partial_t \partial_T + \mathcal{O}(\varepsilon^2).$$

Case I: 2:1 channel, let $\chi = 0$

Use $\Omega = \omega_H$ and keep terms up to $\mathcal{O}(\varepsilon)$. Insert the ansatz in (29) with $j_0 = \varepsilon J$. At $\mathcal{O}(1)$ we get

$$(-\omega_d^2 + \omega_J^2)(A e^{i\omega_d t} + \bar{A} e^{-i\omega_d t}) = 0,$$

which enforces the near resonance choice $\omega_d \approx \omega_J$. For (27), the $\mathcal{O}(1)$ terms vanish identically because $a_x^2 \sim \mathcal{O}(1)$ and $g \sim \mathcal{O}(\varepsilon)$.

Next collect the coefficients of $e^{i\omega_d t}$ at $\mathcal{O}(\varepsilon)$ from (29):

$$-2i\omega_d A' - i\gamma_J \omega_d A - 2\omega_d \sigma_J A + \frac{J}{2} = 0.$$

Divide by $2\omega_d$ (replace $\omega_d \rightarrow \omega_J$ at this order) to obtain the *envelope*:

$$A' = -\left(\frac{\gamma_J}{2} + i\sigma_J\right)A + \frac{J}{4\omega_J}. \quad (33)$$

At last, we compute the quadratic drive:

$$a_x^2 = A^2 e^{2i\omega_d t} + 2|A|^2 + \bar{A}^2 e^{-2i\omega_d t}.$$

Insert in (27); the term resonant with $e^{i\Omega t}$ is the one at $2\omega_d \approx \omega_H = \Omega$. Collecting the $e^{i\Omega t}$ pieces at $\mathcal{O}(\varepsilon)$ gives

$$-2i\Omega H' - i\gamma_H \Omega H - 2\Omega \sigma_H^{(2:1)} H - G \frac{A^2}{2} = 0.$$

Divide by $2\Omega \simeq 2\omega_H$ to obtain

$$H' = -\left(\frac{\gamma_H}{2} + i\sigma_H^{(2:1)}\right)H - i \frac{G}{4\omega_H} A^2. \quad (34)$$

Equations (33) and (34) will give the envelope functions. Other nonresonant harmonics average out.

Case II: sum channel with back-coupling $\chi \neq 0$

Now keep the $\chi h a_x$ term in (29) and choose $\Omega = \omega_d - \omega_J$. The product $h a_x$ contains a component

$$(H e^{i\Omega t})(\bar{A} e^{-i\omega_d t}) = (H \bar{A}) e^{-i\omega_J t},$$

and its complex conjugate. Upon detuning and after removing rapidly oscillating pieces, the term resonant with $e^{i\omega_d t}$ is $A \bar{H}$. Collecting terms similar to those in case I yields

$$A' = -\left(\frac{\gamma_J}{2} + i\sigma_J\right)A + \frac{J}{4\omega_J} - i \frac{C}{4\omega_J} A \bar{H}, \quad (35)$$

$$H' = -\left(\frac{\gamma_H}{2} + i\sigma_H^{(\text{sum})}\right)H - i \frac{C}{4\omega_H} A^2. \quad (36)$$

Again, only the resonant combinations survive; all nonresonant harmonics average out at $\mathcal{O}(\varepsilon)$.

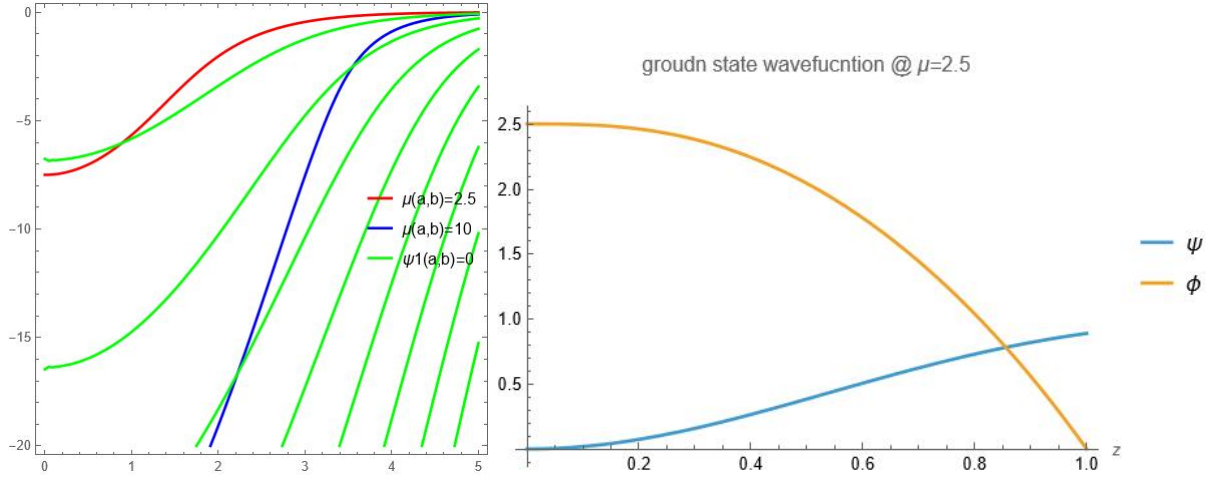


FIG. 1: (Left) Contour plot of given boundary conditions for fixed μ and $\psi^{(1)} = 0$ in the shooting parameters space. Solutions exist at intersecting points. For higher chemical potential (for instant, $\mu = 10$), there exists multiple solutions for excited states. (Right) In our simulation, we use the ground state wavefunctions $\psi(z)$ and $\phi(z)$ for $\mu = 2.5$.

We remark that the steady-state linear response of (33) is $A_\infty = \frac{J}{4\omega_J} \frac{1}{\gamma_J/2 + i\sigma_J}$, which, inserted in (34), gives the growth rate $\Re \lambda_H = -\gamma_H/2 + \frac{|G|}{4\omega_H} |A_\infty|^2$ and the usual 2:1 onset condition. Similar discussion applies to the sum channel. It is expected that the growth rate is negative without driving (decay), but positive with overdriving (blowing up).

V. TIME-CRYSTALLINE PHASE FROM BULK NUMERICS

In this section we provide a concrete numerical example of time-crystalline phase in the holographic superconductor. We outline the numerical procedure as follows:

1. Solve coupled ODEs (4) and (5) for $\{\psi_0, \phi_0\}$ with boundary conditions (6), given a constant chemical potential. To achieve this, we employ a shooting method from the horizon to the boundary. For stability, we tune the initial condensate value to match the source-free boundary condition $\psi^{(1)} = 0$, achieving convergence to within 10^{-4} relative error, see Fig. 1.
2. Compute the lowest QNMs: $\omega_J^{\text{QNM}}, \omega_H^{\text{QNM}}$ via horizon-to-boundary shooting. Define $\omega_{J/H} = \Re \omega^{\text{QNM}}, \gamma_{J/H} = -2\Im \omega^{\text{QNM}}$. For our pick $\mu = 2.5$, one obtains $\omega_H^{\text{QNM}} \approx 0.951 - i1.676$, $\omega_J^{\text{QNM}} \approx 1.633 - i1.304$.

3. Evaluate g and χ using overlaps by normalizing with the weights Y_J and Y_H , yielding $g \approx 0.4876$ and $\chi \approx 557.7$ for the chosen parameters.

4. Insert parameters into the ODEs and solve time-domain evolution by scanning j_0 and ω_d ; verify the subharmonic peak in the spectrum of h .

We remark that the couplings g and χ obtained from step 3 may not be unique but enjoy a scaling symmetry:

$$g \rightarrow \lambda_1 g, \quad \chi \rightarrow \lambda_2 \chi. \quad (37)$$

Then the boundary ODEs (27) and (29) remain the same under the field redefinition:

$$a \rightarrow a/\sqrt{\lambda_1 \lambda_2}, \quad J \rightarrow J/\sqrt{\lambda_1 \lambda_2}, \quad h \rightarrow h/\lambda_2. \quad (38)$$

In practical numerical simulation, we will take advantage of this scaling to normalize the couplings for a clean spectrum.

As shown in FIG. 2, we found that for small driving current, the Higgs mode oscillates at twice the driving frequency (harmonic response). For large driving, nonlinearity leads to envelope growth and distortion. In Fig. 3, a finite number of resonant peaks are observed in the spectra of both the 2:1 and sum channels. These subharmonic peaks, in particular, signify the presence of a time-crystalline phase [15].

VI. DISCUSSION AND CONCLUSION

The projection onto the lowest quasinormal modes (QNMs) provides a controlled one-pole truncation of the bulk dynamics. This approximation is quantitatively reliable in the vicinity of the first plasma resonance and for moderate driving strengths. For stronger driving or when operating away from primary resonances, higher QNMs and couplings among different modes become increasingly relevant. In such regimes, the present framework can be systematically extended by enlarging the QNM basis and repeating the Galerkin reduction, or by reverting to fully backreacted numerical solutions [16]. In our simulation we have ignored the phases occurred in (26) and (28) for simplicity. The imaginary parts of g and χ effectively renormalize the linear damping coefficients and can be absorbed into γ_J and γ_H at leading order. The derivation also straightforwardly adapts to alternative scalar quantizations by interchanging source and vacuum expectation value near the AdS boundary.

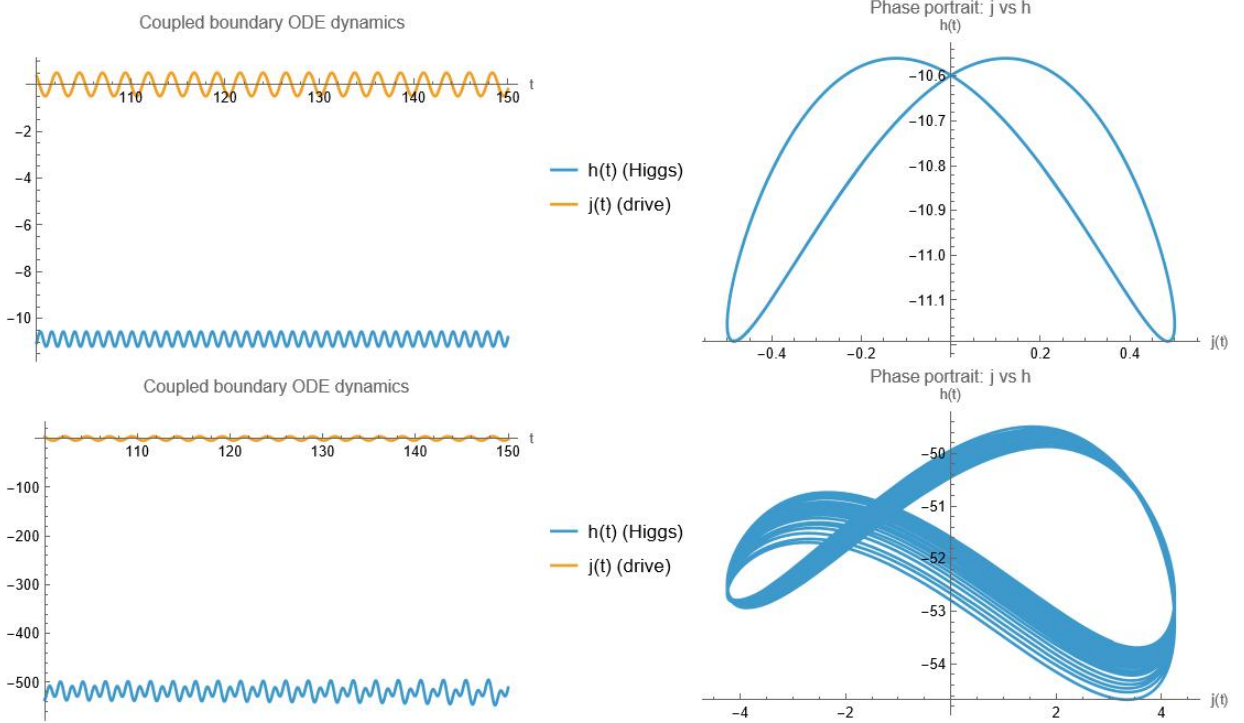


FIG. 2: (Top Left) A typical Higgs mode h responds to small driving current j in sum channel. (Top Right) Phase diagram of j v.s. h shows a closed and stable trajectory. (Bottom Left) Distorted Higgs mode h responds to large driving current j in sum channel, where envelope amplitude is growing and will blow up at later time (not shown), indicating failure of perturbation approach. (Bottom Right) Phase diagram shows uneven and non repeating trajectory. We remark that the amplitudes of $j(t)$ and $h(t)$ have been rescaled for presentation purpose. We only show first 150 sampling points in time domain.

Building on this controlled reduction, we have presented a self-contained derivation of boundary effective ordinary differential equations governing driven, homogeneous dynamics of a single-band holographic superconductor, with all coefficients fixed from first principles and appropriate rescalings. A multiple-scale analysis of these equations predicts robust subharmonic (time-crystalline) responses, in quantitative agreement with numerical simulations. The formalism is readily generalizable to multi-band holographic superconductors, as well as to inhomogeneous or finite-size drive geometries. Extensions incorporating momentum-dependent couplings, finite-size effects, or more realistic lattice structures can be implemented within the same framework [17, 18].

Beyond the minimal setup considered here, several physically motivated directions merit

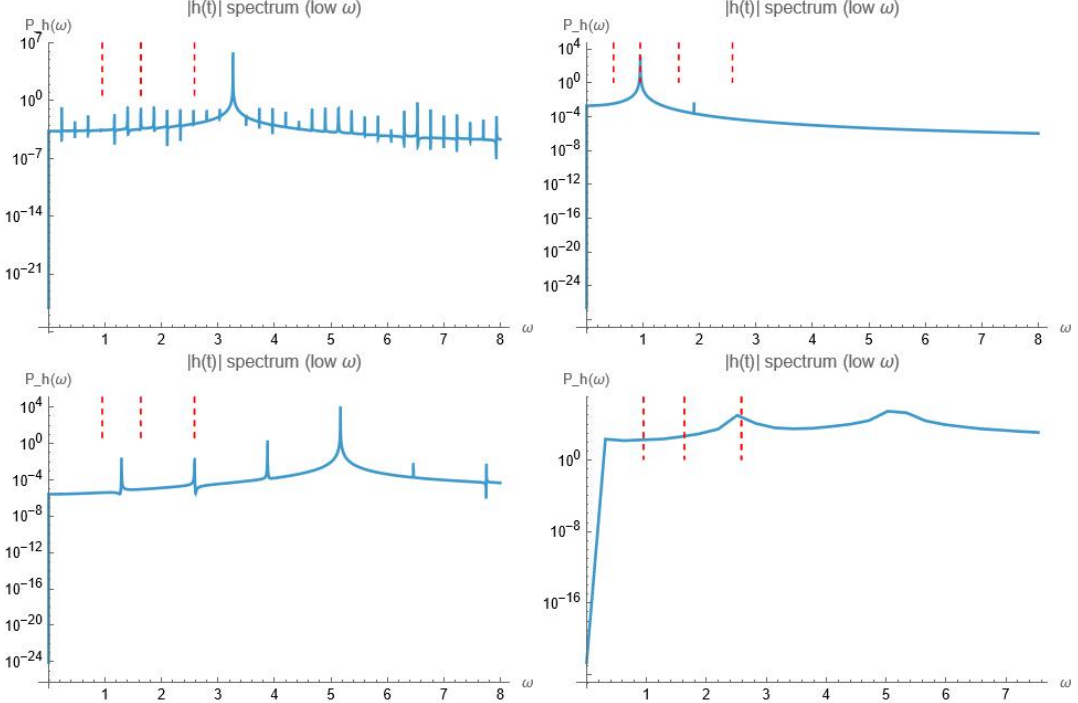


FIG. 3: (Top Left) Power spectrum of Higgs mode in 2:1 channel for $\omega_d = \omega_J$. The vertical red dashed lines indicate ω_H , ω_J , $\omega_H + \omega_J$ from left to right. Among many resonance peaks, the strongest resonance happens at $2\omega_J$. (Top Right) Power spectrum of Higgs mode in 2:1 channel for $2\omega_d = \omega_H$. The extra vertical dashed line (most left) indicates ω_d . The strongest resonance happens at ω_H . (Bottom Left) Power spectrum of Higgs mode in sum channel for $\omega_d = \omega_J + \omega_H$. Resonance happens at integer multiples of $(\omega_J + \omega_H)/2$. (Bottom Right) Power spectrum of Higgs mode in sum channel, but for runaway Higgs amplitude (large driving current). Vanishing subharmonic peaks signify the system has left time-crystalline phase. We note that parameters for this simulation are $\mu = 2.5$, $\omega_H = 0.95$, $\omega_J = 1.63$, $\gamma_H = 3.35$, $\gamma_J = 2.61$, $g = 4.88$, $\chi = 5.58$ (rescaled).

further investigation. Finite-temperature extensions could clarify crossover behavior and the fate of time-crystalline responses near criticality³, while coupling to competing orders—such as charge density waves or nematic phases—may generate richer dynamical phase diagrams. Such studies could establish connections to experimentally observed nonequilibrium phe-

³ We thank [20] for pointing out their holographic approach on Anderson-Higgs mechanism, where a crossover of Higgs mode was observed at about half T_c . We do not expect to observe this crossover since we have chosen the fixing chemical potential such that boundary temperature is not far away from T_c .

nomena in bilayer graphene, moiré materials, and related strongly correlated systems [19]. These extensions may also shed light on the interplay between driven superconductivity and other collective modes in complex quantum materials.

More broadly, by applying holographic methods to time-crystalline behavior previously observed in simulated lattice high- T_c superconductors, this work highlights the utility of gauge/gravity duality in capturing intrinsically nonperturbative dynamics inaccessible to weak-coupling approaches. The predicted subharmonic responses closely resemble the experimental signatures observed in optically pumped cuprates, suggesting that holographic models can serve as effective simulators for ultrafast spectroscopy. Future directions include incorporating quantum noise through stochastic holography to assess stability against decoherence, as well as explicitly modeling coupling to external baths to realize open-system time crystals. Ultimately, these insights may inform the design of quantum devices that exploit broken time-translation symmetry to enhance coherence times or enable novel Floquet engineering protocols.

Acknowledgments

Early work of this project has been presented in the NSYSU (Taiwan) and we thank Prof. Dimitrios Giataganas and Prof. Chia-Yi Ju for inspiring discussions. This work was supported in part by Taiwan’s Ministry of Science and Technology under grant numbers NSTC 112-2112-M-033-003-MY3, NSTC 114-2811-M-033-004 and NSTC 114-2112-M-033-011, and by the National Center for Theoretical Sciences (NCTS). The authors acknowledge the use of the ChatGPT and Grok for assistance with language editing, code formatting, and manuscript organization. All scientific content, derivations, and conclusions were developed and verified by the authors. Numerical calculations were performed using MATHEMATICA, with additional analysis carried out using custom Python scripts.

Appendix A: Damping from horizon flux and Rayleigh functional

This appendix shows explicitly why the dissipative terms in the reduced ODEs can be encoded by a Rayleigh functional $\mathcal{R} = \frac{1}{2}\gamma_J \dot{a}_x^2 + \frac{1}{2}\gamma_H \dot{h}^2$ with $\gamma = -2 \Im \omega^{\text{QNM}}$ for each channel.

A. Energy balance and radial flux

For a quadratic field theory on a fixed black-brane background, the canonical energy of a homogeneous perturbation Φ is

$$E[\Phi] = \frac{1}{2} \int_0^1 du \left(W |\partial_t \Phi|^2 + P |\partial_u \Phi|^2 + V |\Phi|^2 \right), \quad (\text{A1})$$

with time-kinetic weight $W(u) = \sqrt{-g}(-g^{tt}) \times (\text{index factor})$. Varying the action and using the equations of motion yields the balance law

$$\frac{dE}{dt} = - \left[\mathcal{F}_{\text{rad}} \right]_{u=0}^{u=1}, \quad (\text{A2})$$

where \mathcal{F}_{rad} is the radial energy flux density. For QNM boundary conditions, the boundary source vanishes at $u \rightarrow 0$, and hence at $dE/dt = -\mathcal{F}_{\text{hor}} \leq 0$. Near the horizon, use the Eddington-Finkelstein (EF) time $v = t + \int du/f$. A regular mode behaves as $\Phi \sim e^{-i\omega v}$, which implies a positive ingoing flux $\mathcal{F}_{\text{hor}} > 0$ whenever $\Re\omega > 0$.

B. QNM Wronskian identity and $\gamma = -2\Im\omega$

Write the radial equation in Sturm-Liouville form,

$$(pY')' + (\lambda w - q)Y = 0, \quad \lambda = \omega^2, \quad (\text{A3})$$

with $(p, w) = (f, 1/f)$ for A_x and $(p, w) = (f/u^2, 1/(u^2 f))$ for the Higgs scalar. Multiply by Y^* , subtract the conjugate and integrate:

$$\left[p(Y^*Y' - YY'^*) \right]_0^1 + 2i\Im(\lambda) \int_0^1 du w |Y|^2 = 0. \quad (\text{A4})$$

At $u = 0$ the surface term vanishes due to the boundary condition without source. Using the EF behavior of the initiating $Y \sim (1-u)^{-i\omega/3}$ and $f \simeq 3(1-u)$, the horizon term is evaluated to $-2i\Re\omega |Y(1)|^2$. For small damping, $\Im(\lambda) = 2\Re\omega \Im\omega$, hence

$$-\Im\omega \int_0^1 du w |Y|^2 = \frac{1}{2} |Y(1)|^2. \quad (\text{A5})$$

With the kinetic normalization $\int w |Y|^2 = 1$, this gives $-\Im\omega = |Y(1)|^2/2$ and therefore

$$\gamma := -2\Im\omega^{\text{QNM}} = |Y(1)|^2. \quad (\text{A6})$$

C. Matching to Rayleigh dissipation

For a reduced coordinate $q(t)$ with $L = \frac{1}{2}\dot{q}^2 - \frac{1}{2}\omega^2q^2$, Rayleigh's functional $\mathcal{R} = \frac{1}{2}\gamma\dot{q}^2$ produces $\ddot{q} + \gamma\dot{q} + \omega^2q = 0$ and power loss $P_{\text{diss}} = -\gamma\dot{q}^2 = -2\mathcal{R}$. Using the mode truncation $\Phi(u, t) = q(t)Y(u)$ and normalization $\int w|Y|^2 = 1$, the bulk flux identity implies $\mathcal{F}_{\text{hor}} = \gamma\dot{q}^2$ with $\gamma = -2\Im\omega$. Hence, the Rayleigh functional in the reduced ODEs exactly reproduces the horizon energy sink implied by the QNM imaginary parts.

- [1] A. Shapere and F. Wilczek, Phys. Rev. Lett. **109**, 160402 (2012) doi:10.1103/PhysRevLett.109.160402
- [2] F. Wilczek, Phys. Rev. Lett. **109**, 160401 (2012) doi:10.1103/PhysRevLett.109.160401
- [3] P. Bruno, Phys. Rev. Lett. **111**, no.7, 070402 (2013) doi:10.1103/PhysRevLett.111.070402
- [4] D. V. Else, B. Bauer and C. Nayak, Phys. Rev. Lett. **117**, no.9, 090402 (2016) doi:10.1103/PhysRevLett.117.090402
- [5] D. V. Else, C. Monroe, C. Nayak and N. Y. Yao, Ann. Rev. Condensed Matter Phys. **11**, no.1, 467-499 (2020) doi:10.1146/annurev-conmatphys-031119-050658
- [6] K. Giergiel, T. Tran, A. Zaheer, A. Singh, A. Sidorov, K. Sacha and P. Hannaford, New J. Phys. **22**, 085004 (2020) doi:10.1088/1367-2630/aba3e6
- [7] G. Homann, J. G. Cosme, and L. Mathey, Phys. Rev. Res. **2**, 4, 043214 (2020) doi:10.1103/PhysRevResearch.2.043214
- [8] R. Kleiner, X. Zhou, E. Dorsch et al. Nat Commun **12**, 6038 (2021) doi:10.1038/s41467-021-26132-y
- [9] D. Nevola, N. Zaki, J. M. Tranquada et al. Phys. Rev. X **13**, 011001 (2023) doi:10.1103/PhysRevX.13.011001
- [10] H. P. Ojeda Collado, G. Usaj, C. A. Balseiro et al. Phys. Rev. Res. **3**, 4, L042023 (2021) doi:10.1103/PhysRevResearch.3.L042023
- [11] P. E. Dolgirev, A. Zong, M. H. Michael et al. Commun Phys **5**, **234** (2022) doi:10.1038/s42005-022-01007-w
- [12] S. A. Hartnoll, C. P. Herzog and G. T. Horowitz, JHEP **12**, 015 (2008) doi:10.1088/1126-6708/2008/12/015

- [13] X. Huang, S. Sachdev and A. Lucas, Phys. Rev. Lett. **131**, no.14, 141601 (2023) doi:10.1103/PhysRevLett.131.141601
- [14] D. N. Basov, R. Averitt and D. Hsieh, Nat. Mater. **16**, 1077-1088 (2017) <https://doi.org/10.1038/nmat5017>
- [15] A. Greilich, N. E. Kopteva and V. L. Korenev et al. et al. Nat. Commun. **16**, 2936 (2024) doi:10.1038/s41467-024-53147-6
- [16] S. A. Hartnoll, C. P. Herzog and G. T. Horowitz, Phys. Rev. Lett. **101**, 031601 (2008) doi:10.1103/PhysRevLett.101.031601
- [17] W. Y. Wen, M. S. Wu and S. Y. Wu, Phys. Rev. D **89**, no.6, 066005 (2014) doi:10.1103/PhysRevD.89.066005
- [18] X. K. Zhang, X. Zhao, Z. Y. Nie, Y. P. Hu and Y. S. An, Phys. Lett. B **868**, 139684 (2025) doi:10.1016/j.physletb.2025.139684
- [19] S. Y. Frank Zhao et al. Science **382**, 1422-1427 (2023) doi:10.1126/science.abl8371
- [20] H. S. Jeong, M. Baggioli, K. Y. Kim and Y. W. Sun, JHEP **03**, 206 (2023) doi:10.1007/JHEP03(2023)206